IEEE Access
Multidisciplinary | Rapid Review | Open Access Journal

Received March 31, 2020, accepted April 22, 2020, date of publication April 29, 2020, date of current version May 15, 2020.

Digital Object Identifier 10.1109/ACCESS.2020.2991358

Design and Manufacturing of Super-Shaped Dielectric Resonator Antennas for 5G Applications Using Stereolithography

VITO BASILE[1], MARCO GRANDE[2], VALERIA MARROCCO[1], DARIO LANEVE[2], SAVINO PETRIGNANI[2], FRANCESCO PRUDENZANO[2], AND IRENE FASSI[3]

[1]STIIMA CNR, Institute of Intelligent Industrial Technologies and Systems for Advanced Manufacturing, National Research Council, 70124 Bari, Italy
[2]Politecnico di Bari, 70125 Bari, Italy
[3]STIIMA CNR, Institute of Intelligent Industrial Technologies and Systems for Advanced Manufacturing, National Research Council, 20133 Milano, Italy

Corresponding author: Vito Basile (vito.basile@stiima.cnr.it

This work was supported by the STIIMA-CNR Institute through the PAnteBAM: Young Ideas–STIIMA GRANT 2018 Project.

ABSTRACT In this work, the inverted micro-Stereolithography (SLA) is used to show the potential of such additive manufacturing (AM) technology at prototyping super-shaped dielectric resonator antennas (S-DRAs) rapidly and accurately. The S-DRAs, which exhibit 3D complex geometries, were designed to operate at 3.5 GHz, suitable for the assessment of 5G communications in the mid band. Initially, a cross-starred-shaped S-DRA was designed and manufactured via the inverted micro-SLA by means of a photopolymer resin as material. As no information about the used material was available from literature and supplier, the dielectric properties of the photopolymer resin were characterized. Moreover, in the view of challenging further the SLA capability, several prototypes, based on the cross star shaped geometry but exhibiting a twist of variable angles along the longitudinal axis, were fabricated and tested. In order to compare the antennas performance in relation to the material volume and sizes, rectangular and cylindrical DRAs were also realized using same material and technology. Scattering parameter S_{11}, gain, bandwidth (BW), efficiency and co- and cross-polarization of all antennas were measured. The experimental results showed that twisted S-DRAs exhibit same performance of the basic cross-starred-shaped antenna, due to the invariance to symmetry of the basic Gielis geometry. The measured gain is about 2.5 dB over a range of 1 GHz in the frequency range of interest; the BW measured for all S-DRAs is about 10%, whereas the efficiency is about 80% at 3.5 GHz. Finally, better performance in terms of bandwidth is shown by the S-DRAs, considering their dramatic volume reduction (∼85%) compared to classic rectangular and cylindrical DRAs and other DRA examples already reported in the state of the art.

INDEX TERMS Additive manufacturing, dielectric resonator antenna, stereolithography, 5G communication.

I. INTRODUCTION

Dielectric Resonator Antennas (DRA) are excellent candidates for higher frequency application [1], [2] as they exhibit higher radiation efficiency than antennas based on metals and absence of conduction losses. DRAs were usually designed by using dielectric materials with both low and high relative dielectric permittivity ε_r, although high values entail a decrease of the bandwidth (BW). Therefore, especially for 5G mid band applications, a trade-off between radiation and bandwidth requirements is envisaged to accomplish good overall DRA performance. This issue has recently found an interesting solution in the exploitation of low ε_r materials.

A first attempt to select low ε_r materials suitable for microwave range applications was proposed by Kumar and Gupta [3], which evaluated several dielectric materials, such as different type of Rogers. Other authors proposed the dielectric material FR4 [4]–[6]. Indeed, as pointed out by the same authors in [4]–[6], the proposed 3D fractal DRAs were

The associate editor coordinating the review of this manuscript and approving it for publication was Mingjian Li.

TABLE 1. Comparison of technologies for DRA fabrication.

Fabrication Technology	Typical geometries	Materials	Auxiliary equipment & set-up	Ref
Turning [a]	Axial Symmetry with limitations [b]	Metals, polymers, ceramics, composites	Fixtures, axes zero-ing, tools setup [c]	[5]
Milling [a]	3D complex geometries with limitations [b]	Metals, polymers, ceramics, composites	Fixtures, axes zero-ing, tools setup [c]	[9]
Abrasive Water Jet (AWJ) + Assembly	Assembled stack of thin 2D-shaped slices	Metals, polymers, ceramics, composites	Fixtures, axes zero-ing	[6]
Laser cutting + Assembly	Assembled stack of thin 2D-shaped slices	Metals, polymers, ceramics, composites	Fixtures, axes zero-ing	[10]
Stereolithography (SLA)	3D complex [c]	Photopolymers & ceramics	UV curing post-processing	[11]
Fused Deposition Modeling (FDM)	3D complex [d]	Thermoplastics & composites	-	[12]
Polymer jetting Modeling (PJM)	3D complex [d]	Thermoplastics and photopolymer	-	[13], [14]
Injection molding (IM)	3D complex [d]	Thermoplastics, ceramics (CIM)	Mould design & production; IM machine set-up	[15]

[a] Often also drilling is required
[b] Depending on the machine degrees-of-freedom.
[c] Multiple placements of the workpiece could be required.
[d] Sculptured surfaces, multi-facets, curvilinear features, thin walls, 3D-path holes.

manufactured by means of traditional subtractive technologies and a final stack assembly of FR4 disks.

Indeed, the fabrication of low ε_r material based DRAs featuring 3D complex geometries can be quite troublesome. Therefore, alternative manufacturing approaches are recommended.

In the last decade, additive manufacturing (AM) technologies have shown high versatility and flexibility in a variety of applications. In particular, they are becoming very promising for the fabrication and high-customization of prototypes and low batches of compact electronic and telecommunication devices, such as antennas, dielectric resonator antennas (DRAs), sensors, electronic circuits, aimed at realizing next-generation devices with improved performance [7], [8]. Table 1 reports a comparison of technologies suitable for the fabrication of dielectric resonator antennas (DRAs).

Typical subtractive manufacturing technologies, such as turning and milling, are capable of machining almost all kinds of materials, but they have some limitations in fabricating 3D complex geometry. In addition, these technologies require complex and time-consuming setup operations. Other non-conventional technologies like laser cutting and abrasive waterjet (AWJ) have been used to fabricate DRAs, as well. However, final assembly operations are often required to obtain the final antenna, and so, eventual consequent loss of geometric accuracy may affect also the device performance. Concerning injection molding (IM), this technology is generally used for mass production, since it is capable of realizing high production volume of complex 3D geometry by exploiting a pre-designed and machined mold. Nonetheless, IM is also typically characterized by high time-to-market and high investment, particularly for the mold fabrication. In relation to the additive manufacturing (AM) technologies reported in table 1, stereolithography, (SLA), fused deposition modelling (FDM) and polymer jetting (PJM) exploit dielectric materials. For this reason, they are excellent candidate for DRA fabrication exhibiting high complex 3D geometries. Differently from subtractive technologies and IM, AM ones have the remarkable advantage of being completely digitalized, thus allowing to realize parts starting directly from their 3D CAD virtual models. They do not require setup operations and they are a smart choice for fast prototyping, and for small production lots of devices and components before their final mass production.

However, the selection of the proper 3D printing technology is of paramount importance, as different AM processes lead to different quality of the final component. To this aim, some key factors must be taken into account: material characterization, device geometry and complexity, target performance. In [16], Semeoni *et al.* proposed the design and the fabrication of a four pseudo-vertexes cross-starred S-DRA based on the widely acknowledged Gielis superformula [17], [18]. The antenna, designed to operate around 8 GHz, was made by polyvinyl chloride (PVC) thermoplastic, having $\varepsilon_r = 2.8$ and negligible loss tangent, and fabricated by extrusion. The experimental results related to single feed condition showed that a gain of 4.8 dBi and a BW=74 % could be successfully accomplished. A recent example concerning the adoption of fused deposition modeling (FDM) to fabricate DRAs having different shapes was proposed in [19], [20], [12]. Specifically, rectangular, spherical, triangular [19], and 3D quadrupole-shaped DRAs for WI-LAN and 5G communications were manufactured by means of poly lactic acid (PLA), a biodegradable thermoplastic featuring $\varepsilon_r = 3.48$ and negligible loss tangent [20], [12]. Additionally, in [12], the same 3D quadrupole shaped geometry was also fabricated by means of SLA, considering photopolymer resin as material. The main objective of such study was to demonstrate how two different AM technologies, based on different processes and materials, affected the overall DRAs performance: specifically, surface roughness and dimensional accuracy of the final components were put in relation to scattering parameters $S_{11}$and gain.

In the present work, the inverted micro-Stereolithography (SLA) is applied to the manufacturing of 3D super-shaped DRAs prototypes suitable for 5G communications related to mid band (sub-6GHz band). The motivation of the present study is actually twofold: first, it addresses the challenge of producing complex and accurate Gielis-based S-DRAs as entire complete structure by using inverted micro-SLA; second, it enables the fabrication of S-DRAs with improved performance but with reduced size, volume and amount of material, compared to standard DRA geometries (cubic and cylindrical).

To accomplish these goals, several S-DRA prototypes, designed to operate in the 3.5 GHz band to meet 5G specifications, were designed and produced. A photopolymer based on methacrylic acid esters, referred as photopolymer resin,

TABLE 2. Symbols with units.

Symbol	Quantity	Units
f	Frequency	Hz
f_r	First resonant frequency	Hz
BW	Bandwidth	%
G	Gain	dBi
V	Volume	cm^3
ε_r	Relative dielectric constant	-
tan(δ)	Tangent loss	-
S_{11}	Scattering parameter	dB

was chosen as material. Since no information was available for dielectric permittivity and loss tangent of the photopolymer resin, measurements were performed to evaluate these parameters in the frequency range of interest. Additionally, other S-DRAs exhibiting a twist with variable angle (45, 90, 135, 180, 270 and 360 degrees) along the longitudinal axis were fabricated, tested and measured by means of a Vector Network Analyzer (VNA) and an anechoic chamber. Finally, rectangular and cylindrical DRAs were also realized using SLA and same material, in order to compare their performance.

The paper is organized as follows. Section II.A comprises the geometrical model description of the basic cross-starred super shaped DRA based on Gielis superformula, its design and optimization; a comparison of the performance among cylindrical (C-DRA), rectangular (R-DRA) and cross-star shaped S-DRA is also carried out by means of Finite Element Method (FEM) simulations implemented via COMSOL Multiphysics ©. Section II.B reports the analytical formulas and the geometrical models about the twisted S-DRAs. Section III focuses on the principle of operation of inverted micro-SLA, along with process details and fabrication issues. Section IV concerns the characterization of the dielectric properties of the photopolymer resin and the measurements of the DRAs samples; a discussion of results about DRAs performance in relation to the fabrication process is also included. Finally, Section V reports the conclusion. For sake of clarity, Table 2 reports the list of symbols related to some physical parameters and dielectric characterization that will be used throughout the manuscript.

II. SUPER-SHAPED DRAs: DESIGN AND FEATURES

A. S-DRA BASIC GEOMETRICAL MODEL, DESIGN AND OPTIMIZATION

The starting point for the design of an S-DRA is the following Gielis superformula [17], [18]:

$$r_d(\varphi) = \frac{1}{\sqrt[n_1]{[|\frac{1}{a}\cdot cos\frac{m\cdot\varphi}{4}|^{n_2} + |\frac{1}{b}\cdot sin\frac{m\cdot\varphi}{4}|^{n_3}]}} \quad (1)$$

TABLE 3. Dimensions (R-DRA & C-DRA) and parameters of basic S-DRA.

C-DRA		R-DRA	
Diameter [mm]	Height [mm]	Side □ [mm]	Height [mm]
29	31.1	30	26.8

S-DRA						
a	b	m	n_1	n_2	n_3	Height
[-]	[-]	[-]	[-]	[-]	[-]	[mm]
1.6	1.6	4	10	30	30	25

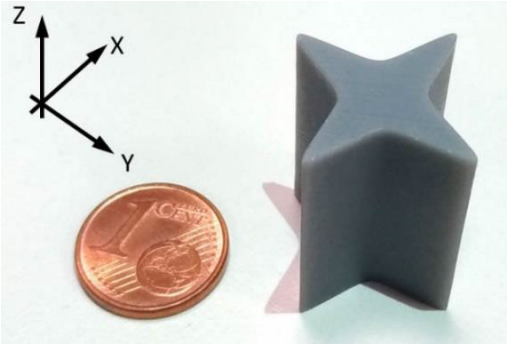

FIGURE 1. Cross-starred shape DRA having parameters reported in table 1.

where $r_d(\phi)$ is the radial coordinate which defines a closed curve on the plane, φ is the polar angle coordinate which can assume any value in the interval $[0, 2\pi]$, while a, b, m, n_1, n_2 and n_3 are positive real numbers, where a, b $\neq 0$. In relation to equation (1), in this work, the fundamental geometry comprising the four-vertex-supershape (m=4) characterized by two planes of symmetry, normal to each other, is considered (Figure 1). The design optimization of this basic S-DRA antenna was performed by finite element method (FEM) and compared with an R-DRA and a C-DRA [21]. The S-DRA structure was designed to operate at a central operational frequency of 3.5 GHz; in order to do so, multi-parameter analysis was carried out to obtain optimized Gielis formula parameters reported in table 3. Moreover, the height H and dimensions of C-DRA and R-DRA are also described in table 3 [21]. As explained later in section IV, the dielectric permittivity value of the material considered for the antenna design was the actual ε_r of the Grey resin V04, used for the antenna fabrication.

FEM analyses of the basic S-DRA and of the cylindrical and rectangular DRAs were performed, in order to compare the antenna performance in terms of scattering parameter S_{11}, efficiency and gain (Figure 2a-b-c, respectively).

Figure 2d reports the radiation pattern at the operation frequency 3.5 GHz of the S-DRA. All DRAs display similar performance in terms of S_{11} (about -20 dB at 3.5 GHz), a bandwidth of BW = 28%; the gain is about 4.4 dB and an efficiency of about 97% can be obtained at 3.5 GHz.

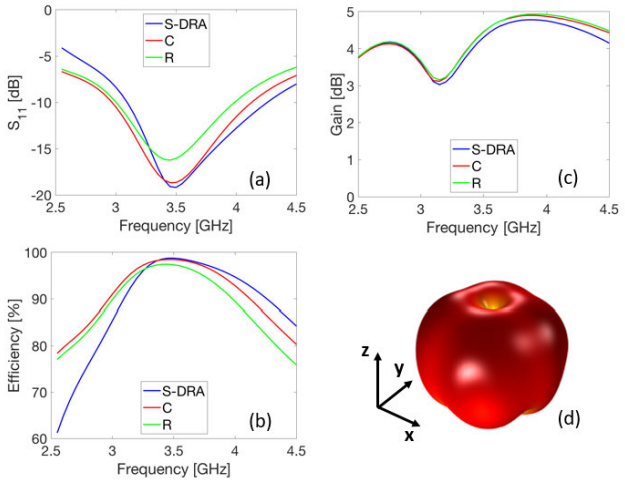

FIGURE 2. (a) Scattering parameter S_{11}, (b) efficiency and (c) gain related to the Cross-starred shape S-DRA having parameters reported in table 1, along with C-DRA and R-DRA; (d) radiation pattern of the S-DRA at 3.5 GHz. The radiation patterns for the C-DRA and R-DRA are similar to the radiation pattern of the S-DRA.

B. TWISTED S-DRAs: ANALYTICAL FORMULAS AND GEOMETRICAL MODELS

Since one of the aims of the present work is to test inverted micro-SLA capability at manufacturing the antennas, a modified and more complex geometry has been conceived for S-DRA. In particular, the basic super-shape, defined by equation (1) considering four pseudo-vertexes (m=4) and parameters reported in Table 3, was modified applying a torsion, indicated by the parameter γ, linearly distributed along the longitudinal z-axis.

The torsion can be mathematically formalized by introducing the new polar coordinate φ', which takes into account the rotation of the cross-section along the z-axis:

$$\varphi'(z) = \varphi + \frac{\gamma}{H} \cdot z \quad 0 < z < \mathrm{H} \tag{2}$$

By substituting the equation (2) into equation (1), the Gielis superformula is adjusted to describe the entire 3D geometry in all directions:

$$r_d(\varphi, z) = \frac{1}{n_1 \sqrt{[|\frac{1}{a} \cdot \cos(\frac{m\mathrm{H} \cdot \varphi + \gamma \cdot z}{4 \cdot H})|^{n_2} + |\frac{1}{b} \cdot \sin(\frac{m \cdot H \cdot \varphi + \gamma \cdot z}{4 \cdot H})|^{n_3}]}} \tag{3}$$

In order to verify the effectiveness of the twist phase displacement, several S-DRAs based on the modified Gielis superformula (3) have been fabricated and measured. Starting from the fundamental Gielis super-shape (equation (1) with m=4), five initial S-DRAs geometries, expected to operate at 3.5 GHz, are realized by applying different twist angles $\gamma = 0, 90, 180, 270, 360$ degrees along the z-axis, therefore considering integer multiples of 360/m=90 degrees. In order to "brake" this symmetry and its angular periodicity, the twist γ should be a non-integer multiple of 90 degrees i.e. its half. Therefore, two additional S-DRAs have been fabricated considering twist angles of 45° and 135°.

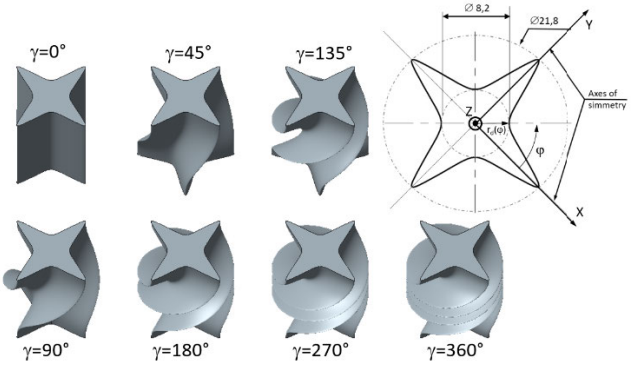

FIGURE 3. S-DRA 3D models with different twist angles γ. Top right: Gielis cross-section drawing with polar coordinates and main dimensions.

III. SUPER-SHAPED DRAs: FABRICATION AND MEASUREMENTS

A. S-DRAs 3D GEOMETRIC MODELING

The virtual solid 3D models of all S-DRAs have been generated by 3D CAD software Solidworks release 2017, exploiting the equation (3) according to the following procedure. First, the simplified four pseudo-vertexes cross-starred-shaped geometry on the x-y plane has been adopted for a solid straight extrusion and, then, a twist transformation has been applied along the overall height of the S-DRA according to equations (2) and (3). The 3D solid geometry has been exported to standardized STL format (Stereolithography format, also referred as "Standard Triangulation Language"), using higher quality parameters (minimum chord height and maximum angle control) to achieve the best accuracy of the geometry representation and interoperability between software. Figure 3 shows the 3D models of S-DRAs and main dimensions of the Gielis cross-section.

These models are the mathematical representation of the 3D geometries provided as the input information for the AM machine. In addition to S-DRAs, cylindrical (C-DRA) and rectangular (R-DRA) dielectric resonator antennas were modelled using the same 3D CAD software.

B. SLA TECHNOLOGY: PRINCIPLE OF OPERATION AND PROCESS PARAMETERS

The SLA technology is based on the polymerization of a liquid monomer mixture induced by a UV-laser light source.

In particular, as the laser spot size is generally less than hundreds of microns in diameter, the final 3D structures display high dimensional accuracy and surface finishing. Especially for 3D complex geometries, comprising sculptured surfaces, multi-facets and curvilinear features, thin walls, etc., the inverted micro-SLA allows to fabricate solid structures, thus avoiding fractures, presence of voids and air gaps, and, ultimately, simplifying, to a certain extent, the final device assembly. Thanks to these features, SLA also holds the potential for down-scaling the antenna sizes, and, as such, it may be an excellent candidate to DRAs dedicated to the emerging 5G mm-wave applications (high band).

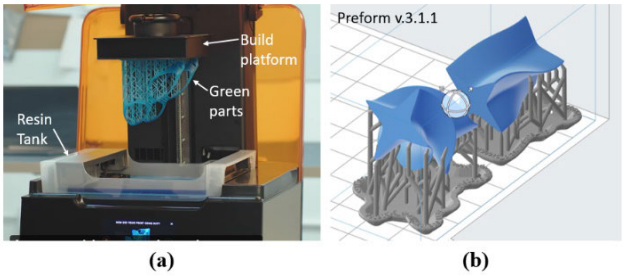

FIGURE 4. SLA fabrication. a) SLA Formlabs Form3 printer. b) Pre-processing with Preform slicer software.

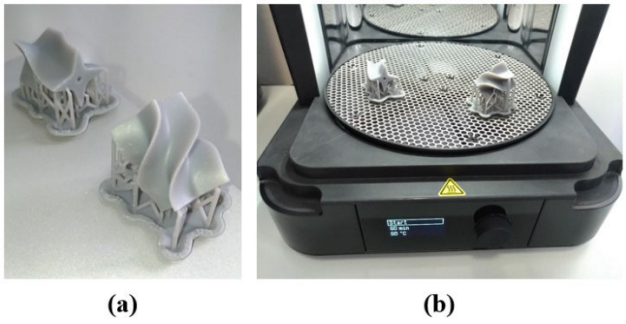

FIGURE 5. SLA samples and post-processing. a) Green parts with supports after 3D printing. b) Samples into the UV-curing machine.

Figure 4 shows the 3Dprinter Formlabs Form3, which implements the inverted (bottom-up) micro-SLA used for the present DRAs fabrication.

The 3Dprinter has a build volume of 145 × 145×185 mm and the light source is a class 1 violet laser operating at a wavelength $\lambda = 405$ nm with a power of 250 mW. The laser spot diameter allows to accomplish a minimum feature size of 85 μm. The photopolymer considered in the present study is a Formlabs Grey resin, release V04 [12], [22], which is a mixture composed by a methacrylic acid esters monomer, a photo-initiator, a terminator and color pigments [23]. The mixture is contained into a resin tank with a transparent bottom.

The UV laser spot is located below the resin tank and impinges onto the transparent bottom, thus triggering the polymerization reactions. As the laser spot moves following a path (generated by processing the STL of the 3D model described in section III.A), the mixture surface solidifies point by point. The positioning resolution is equal to 25 μm along the XY plane, while it can be equal to 100, 50 or 25 μm (layer thickness setting) along the z-axis. In order to fabricate all DRAs, a layer thickness of 25 μm was set to achieve the highest dimensional resolution and accuracy. The build platform, indicated in Figure 4a, is able to move upward along a linear z-axis. At each iteration, a liquid meatus is formed between the layer cured at the previous step, attached to the build platform, and the bottom of the resin tank. When the current layer curing is complete, it is detached from the bottom of the resin tank by the peeling mechanism. The process is then repeated each time lifting up the build platform by the set layer thickness, until the end of the printing. It is worth stressing that the peeling mechanism is one of the most sensitive steps toward a successful SLA fabrication.

Therefore, in order to preserve the geometrical integrity of each cured layer (and final part dimensional accuracy), low detachment forces should be applied. This latter objective can be pursued by an optimal 3D placement (orientation) of the part within the build volume during the printing. Part orientation affects deeply the part stability, surface finishing, printability and processing time. It also affects its mechanical properties since the slicing results in anisotropy of the printed part. Therefore, the 3D placement was accurately chosen.

Supports and layer paths were automatically generated by the slicer software Preform release 3.1.1 as showed in Figure 4b. After the print, the samples need to be subjected to three post-processing steps: washing, manual supports removal and additional UV curing. The washing is required to remove the liquid resin on the printed sample surface and it was made by means of high purity 99.9% isopropyl alcohol (IPA) for 20 minutes into a Formlabs Form Wash machine.

Washed samples are showed in figure 5a. All supports were then gently removed with a cutter. Finally, the samples underwent a further UV curing treatment, performed into a Formlabs Form Cure machine (Figure 5b). The UV curing was made for 60 minutes at a temperature of 60°C by using a UV light at wavelength of $\lambda = 405$ nm and power of 39W.

The additional UV curing aids to improve the DRA strength and increase the part homogeneity and density, so that voids and not polymerized micro-droplets within the mass of the antenna can be drastically reduced. In this application, all parts fabrication required about 1300 layers, resulting in about 30 processing hours and 2.5 post processing hours.

IV. EXPERIMENTAL RESULTS AND DISCUSSION

A. MATERIAL CHARACTERIZATION

Since no information about the relative dielectric permittivity and loss tangent of the Grey Resin V04 photopolymer was available from literature and from the material supplier, we characterized the material in the frequency range of interest (between 2.5 and 4.5 GHz), by means of the open – ended coaxial probe method. In order to proceed with the measurements, two 3Dprinted bricks (SLA1 and SLA2) of the Grey Resin V04 photopolymer were realized via inverted micro-SLA process. The brick dimensions were 60 × 60×30 mm: the two samples, SLA1 and SLA2, underwent different post-processing curing time. Indeed, SLA1 was cured for 60 min at 60°C, while SLA2 was treated for 90 min at 60°C. The following Table 4 reports the data concerning the average values of the measured relative dielectric permittivity and loss tangent for both samples. The values reported in table 4 show that no relevant differences have been introduced by adding

TABLE 4. Measurements of relative dielectric permittivity and loss tangent.

Sample	Epsilon_real ε_r	Loss Tangent tan(δ)
SLA1	2.7060	0.0027
SLA2	2.6880	0.0030

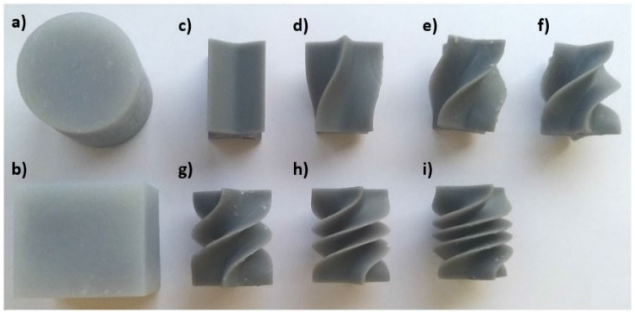

FIGURE 6. DRAs samples made of photopolymer Grey resin V04 and manufactured via SLA. a) C-DRA; b) R-DRA; S-DRAs: c) $\gamma = 0$; d) $\gamma = 45°$; e) $\gamma = 90°$; f) $\gamma = 135°$; g) $\gamma = 180°$; h) $\gamma = 270°$; i) $\gamma = 360°$.

more post-curing time; hence, the shorter post-processing duration can be conveniently applied to the samples.

The manufactured S-DRAs, cylindrical and rectangular DRAs are reported in figure 6.

It can be noticed that the corners of all DRAs are well defined and their surface appears smooth and compact, due also to the post-processing treatments.

B. DRA MEASUREMENTS AND EXPERIMENTAL RESULTS

All the antennas were characterized considering single point feeding through a coaxial cable. In order to insert the coaxial cable within each DRA, a hole of 1.8 mm in diameter and 14 mm depth was realized at the bottom of each DRA. Subsequently, each antenna was located onto a 1.4 mm thick FR4 substrate, with copper-coated backside. A hole was also drilled in the substrate so that the cable belonging to SMA connector could enter the antenna body. The SMA connector was soldered onto the backside of the substrate. In order to fix the antenna, a double-side adhesive tape was used. In this way, it was possible to excite and measure each sample by using the same substrate and coaxial cable length, and so to obtain more reliability and uniformity of the measurements. The DRAs antenna assembly with feed is showed in figure 7, inside the anechoic chamber.

Scattering parameter S_{11} measurements of all assembled DRAs were performed by means of a Vector Network Analyzer (Agilent Technologies, N9917A) and reported in Figure 8.

The S_{11} plot referred to the monopole feed (black line) exhibits a dip around 3.8 GHz. The ripples are present in all curves and are due to soldering imperfection of the SMA connector-substrate interface and to the coaxial feed length. S_{11} plots referred to the S-DRAs show a dip at about 3.2 GHz.

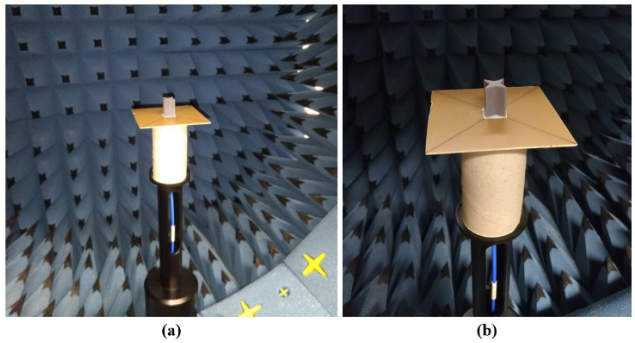

FIGURE 7. Measurements on DRAs. a) Positioning inside the anechoic chamber StarLab by SATIMO; b) Detail of the S-DRA (sample without twist $\gamma = 0$).

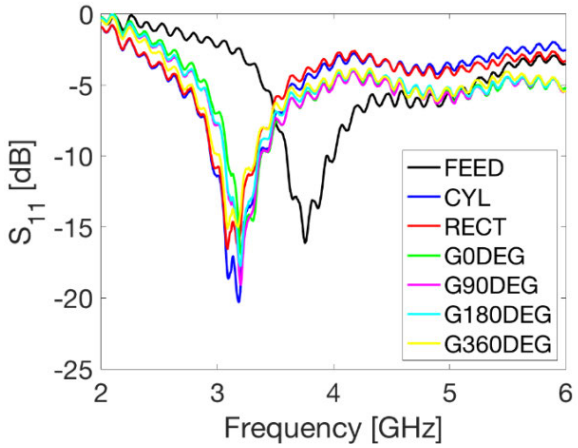

FIGURE 8. Scattering parameter S_{11} measured by means of VNA.

These results witness the invariance of the symmetry along z-axis characterizing the Gielis geometry, although a slight difference of their intensity can be observed. In particular, the S-DRAs twisted by 90° and 180° (pink and cyan lines, respectively), and the original cross-starred S-DRA (indicated by G0°, green line) display about -20 dB, while the S-DRA featuring a twist of 360° (yellow line) exhibits about -15 dB. The cylindrical and rectangular DRAs (blue and red lines, respectively) show a dip at 3.2 GHz, but with different S_{11} intensity (-21 dB for C-DRA and -18 dB for R-DRA).

The gain of each DRA was measured in the anechoic chamber and reported in Figure 9a, while the efficiency is shown in Figure 9b. In particular, all S-DRAs display a gain of about 2.5 dB over a range of about 1 GHz (3-4 GHz), whereas the C-DRA and R-DRA show similar gain but slightly higher BW. These results are confirmed by the efficiency plots, which exhibit a maximum of about 80%.

Figure 10 reports the 3D-radiation patterns of the fabricated S-DRAs, which display a monopole-like behavior for all configurations at 3.5 GHz, fully in line with the numerical results (figure 2d).

Finally, Figure 11 shows the co- and cross-polarization plots for all S-DRAs at 3.5 GHz. Concerning co-polarization,

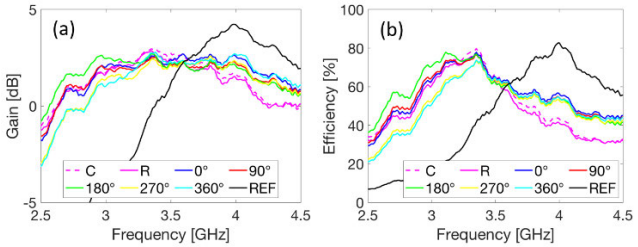

FIGURE 9. a) Gain measurements performed in the anechoic chamber; b) DRAs' efficiency.

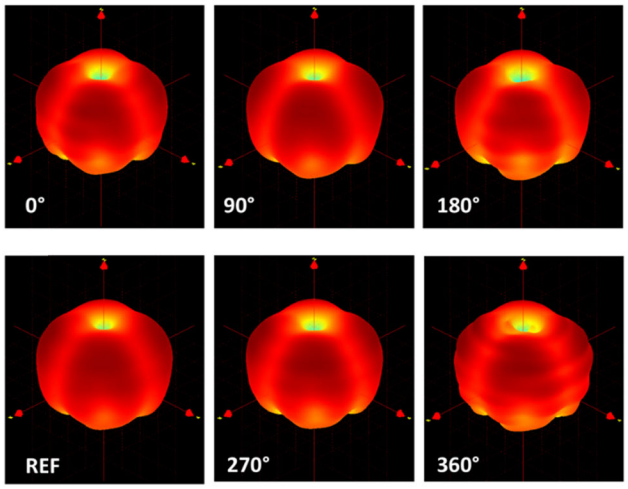

FIGURE 10. 3D radiation patterns of the fabricated S-DRAs at 3.5 GHz.

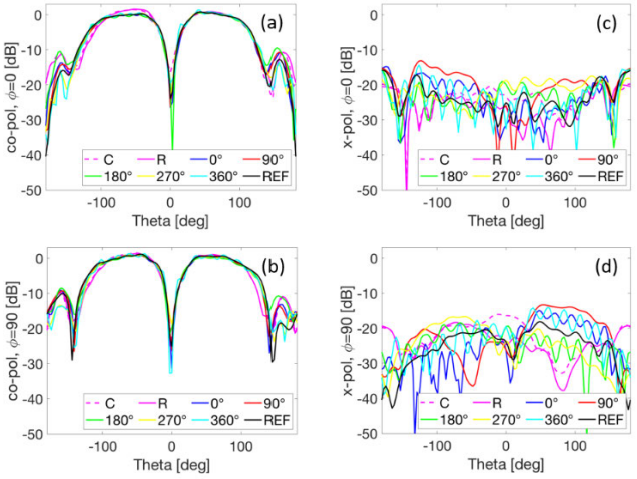

FIGURE 11. (a, b) co-polarization and (c, d) cross-polarization of the fabricated DRAs at 3.5 GHz.

a variation of 5dB for the null and backside lobe directions can be observed for the S-DRAs with $\gamma = 180°$ and $\gamma = 270°$. In relation to the cross-polarization, when the twist is introduced in the basic S-DRA design, a variation of about 10 dB is observed, with a maximum level of about -15 dB.

The following table 5 summarizes the comparison about the performance of different DRAs designs. Taking into account that the frequencies of the fractal DRAs [4] and S-DRA in [16] are in the high band range (> 6 GHz), it can be observed that the proposed S-DRAs have reduced size and volume (smaller up to 85%) but still remarkable BW and gain G.

TABLE 5. Performance Comparison of Different DRA designs from the state of the art.

Geometry		f_r (GHz)	BW (%)	G (dBi)	V (cm^3)
C-DRA [4]	a	3.80	15.00	4.80	33.85
Koch snowflake Iteration 1 [4]	a	6.04	57.20	5.90	18.98
Koch Snowflake Iteration 2 [4]	a	4.57	57.57	6.56	21.09
Fractal Ring [4]	a	6.14	74.23	7.60	15.83
Hal Split Fractal Ring [4]	a	6.00	90.00	8.76	7.91
C-DRA	a	3.50	31.42	4.45	20.54
	b	~3.20	13.10	2.72	
R-DRA	a	3.50	28.57	4.40	24.12
	b	~3.20	11.87	2.45	
S-DRA	a	3.50	32.86	4.30	3.10
	b	~3.20	9.37	2.43	
S-DRA [16]	b	8	74	~4.8	N.A.

a: Numerical result.
b: Experimental measurement.

The S-DRAs volumes reported in table 5 can be calculated by integration of the equation (3) but they can be easily calculated numerically by means of algorithms embedded into the 3D CAD software, applied to the accurate modeling of antennas, as described in section III.A.

V. CONCLUSIONS

In this work, S-DRA samples were fabricated by making use of inverted micro-Stereolithography (SLA). The first intent of the present study was to exploit and show the potential of such technology at fabricating DRAs with high degree of design complexity. To this aim, S-DRAs, designed to operate at 3.5 GHz for 5G applications were fabricated. DRAs prototypes of the basic cross-star shape geometries have been manufactured by considering different twist angles along the vertical axis ($\gamma = 45°, 90°, 135°, 180°, 360°$). The SLA process was thoroughly described, highlighting all issues concerning the 3D printing process. Additionally, since no information about dielectric properties of the photopolymer resin used to fabricate all prototypes was available both from literature and material supplier, the material was characterized to retrieve the relative dielectric permittivity and loss tangent in the frequency range of interest (between 3 and 5 GHz). The printed prototypes showed high surface quality and compactness, due to the smallest layer thickness implemented in the SLA process and to the post-processing procedure. Once all S-DRAs were realized and fed by a coaxial probe inserted within the antennas, they have been

characterized by means of a Vector Network Analyzer and an anechoic chamber. The experimental results showed that gain of about 2.5 dB over a range of about 1 GHz have been accomplished. The goodness of such results was also confirmed by the antennas efficiency, which was about 80% at 3.5 GHz. Furthermore, co- and cross-polarization plots for all S-DRAs at 3.5 GHz showed a variation of 5dB for the null and backside lobe direction for S-DRAs with $\gamma = 180°$ and $\gamma = 270°$. In relation to the cross-polarization, when the rotation was introduced in the basic S-DRA design, a variation of about 10 dB is observed, with a maximum level of about -15 dB. Finally, the comparison among different DRAs designs reported in the state-of-the-art highlights that the performances of the S-DRAs fabricated using inverted micro-SLA and grey resin are remarkable, considering the operation frequency. Furthermore, a drastic reduction of volume and sizes of all antennas can be also appreciated.

ACKNOWLEDGMENT

The authors would like to thank V. Portosi, from Politecnico di Bari, for her support in dielectric properties measurements and Prof. A. D'Orazio, from Politecnico di Bari, for her expertise and scientific contribution to the topic developed in the present context.

REFERENCES

[1] A. Petosa and A. Ittipiboon, "Dielectric resonator antennas: A historical review and the current state of the art," *IEEE Antennas Propag. Mag.*, vol. 52, no. 5, pp. 91–116, Oct. 2010.
[2] S. Keyrouz and D. Caratelli, "Dielectric resonator antennas: Basic concepts, design guidelines, and recent developments at millimeter-wave frequencies," *Int. J. Antennas Propag.*, vol. 2016, Oct. 2016, Art. no. 6075680.
[3] J. Kumar and N. Gupta, "Investigation on microwave dielectric materials for dielectric resonator antennas," *Int. J. Appl. Electromagn. Mech.*, vol. 47, no. 1, pp. 263–272, Jan. 2015.
[4] D. Sankaranarayanan, D. Venkatakiran, and B. Mukherjee, "A novel compact fractal ring based cylindrical dielectric resonator antenna for ultra-wideband applications," *Prog. Electromagn. Res. C*, vol. 67, pp. 71–83, Jan. 2016.
[5] B. Mukherjee, "A novel half hemispherical dielectric resonator antenna with array of slots loaded with a circular metallic patch for wireless applications," *AEU-Int. J. Electron. Commun.*, vol. 69, no. 12, pp. 1755–1759, Dec. 2015.
[6] S. Gupta, P. Kshirsagar, and B. Mukherjee, "A low-profile multilayer cylindrical segment fractal dielectric resonator antenna: Usage for wideband applications," *IEEE Antennas Propag. Mag.*, vol. 61, no. 4, pp. 55–63, Aug. 2019.
[7] F. Calignano, "Overview on additive manufacturing technologies," in *Proc. IEEE*, vol. 105, no. 4, pp. 593–612, Apr. 2017.
[8] E. MacDonald and R. Wicker, "Multiprocess 3D printing for increasing component functionality," *Science*, vol. 353, no. 6307, p. aaf2093, Sep. 2016, doi: 10.1126/science.aaf2093.
[9] M. H. Jamaluddin, R. Sauleau, X. Castel, R. Benzerga, L. Le Coq, R. Gillard, and T. Koleck, "Design, fabrication and characterization of a dielectric resonator antenna reflectarray in Ka-band," *Prog. Electromagn. Res. B*, vol. 25, pp. 261–275, Jan. 2010.
[10] T. A. Denidni and G. Augustin, *Ultrawideband Antennas for Microwave Imaging Systems*. Norwood, MA, USA: Artech House, 2014.
[11] K. F. Brakora, J. Halloran, and K. Sarabandi, "Design of 3-D monolithic MMW antennas using ceramic stereolithography," *IEEE Trans. Antennas Propag.*, vol. 55, no. 3, pp. 790–797, Mar. 2007, doi: 10.1109/TAP.2007.891855.
[12] V. Marrocco, V. Basile, I. Fassi, M. Grande, D. Laneve, F. Prudenzano, and A. D'Orazio, "Dielectric resonant antennas via additive manufacturing for 5G communications," in *Proc. PIERS*, Rome, Italy, Jun. 2019, pp. 174–180.
[13] P. Nayeri, M. Liang, R. A. Sabory-García, M. Tuo, F. Yang, M. Gehm, H. Xin, and A. Z. Elsherbeni, "3D printed dielectric reflectarrays: Low-cost high-gain antennas at sub-millimeter waves," *IEEE Trans. Antennas Propag.*, vol. 62, no. 4, pp. 2000–2008, Apr. 2014.
[14] H. Xin and M. Liang, "3-D-printed microwave and THz devices using polymer jetting techniques," *Proc. IEEE*, vol. 105, no. 4, pp. 737–755, Apr. 2017.
[15] V. K. Palukuru, K. Sonoda, R. Surendran, and H. Jantunen, "BST-COC composite based rectangular dielectric resonator antenna (DRA) for 2.4 WLAN wrist applications," *Prog. Electromagn. Res. C*, vol. 16, pp. 195–205, Jan. 2010.
[16] M. Simeoni, R. Cicchetti, A. Yarovoy, and D. Caratelli, "Plastic-based supershaped dielectric resonator antennas for wide-band applications," *IEEE Trans. Antennas Propag.*, vol. 59, no. 12, pp. 4820–4825, Dec. 2011.
[17] J. Gielis, "A generic geometric transformation that unifies a wide range of natural and abstract shapes," *Amer. J. Botany*, vol. 90, no. 3, pp. 333–338, Mar. 2003.
[18] J. Gielis, "Method and apparatus for synthesizing and analyzing patterns utilizing novel 'super-formula' operator," U.S. Patent 7 620 527 B1, Nov. 17, 2009.
[19] P. Kumar, S. Dwari, Utkarsh, S. Singh, and J. Kumar, "Investigation and development of 3D printed biodegradable PLA as compact antenna for broadband applications," *IETE J. Res.*, vol. 66, no. 1, pp. 53–64, Jan. 2020, doi: 10.1080/03772063.2018.1474140.
[20] P. Kumar, S. Dwari, Utkarsh, and J. Kumar, "Design of biodegradable quadruple-shaped DRA for WLAN/Wi-max applications," *J. Microw., Optoelectron. Electromagn. Appl.*, vol. 16, no. 3, pp. 867–880, Sep. 2017.
[21] S. Petrignani, A. D'Orazio, M. Grande, V. Marrocco, V. Basile, and I. Fassi, "Supershaped dielectric resonator antenna for 5G applications," presented at the IET's Antennas Propag. Conf. (APC), Birmingham, U.K., Nov. 2019.
[22] V. Basile, F. Modica, and I. Fassi, "Analysis and modeling of defects in unsupported overhanging features in micro-stereolithography," in *Proc. ASME Design Eng. Tech. Conf., 21st Design Manuf. Life Cycle Conf., 10th Int. Conf. Micro-Nanosyst.*, Charlotte, NC, USA, vol. 4, Aug. 2016, pp. 1–8, doi: 10.1115/DETC2016-60092.
[23] P. J. Bártolo, Ed., *Stereolithography: Materials, Processes and Applications*. Boston, MA, USA: Springer, 2011, doi: 10.1007/978-0-387-92904-0.

VITO BASILE received the M.Sc. degree in engineering of management from the University of Calabria in 1998, and the master's degree in industrial research from the National Research Council, Italy, in 2003. He was an Assistant Professor of mechanical technologies and production systems with the University of Calabria, Italy, from 1999 to 2002. He gained a relevant industrial experience as a Mechanical Designer, the Technical Manager, and the R&D Project Manager, where he was co-authoring several international patents and winning the IF Award 2012. He joined CNR-ITIA (now CNR-STIIMA) as a Researcher, in 2012. His current research interests include production systems, automation, robotics and manufacturing, and specifically: additive manufacturing technologies, nano-structured materials, and micro-manufacturing technologies.

MARCO GRANDE received the master's degree *(summa cum laude)* in electronic engineering and the Ph.D. degree from the Polytechnic University of Bari, in 2006 and 2010, respectively. Since October 2015, he has been an Assistant Professor of electromagnetic fields with the Polytechnic University of Bari. He is involved in several national and international research projects (US Army and H2020). He has coauthored about 100 publications on international journals and conference proceedings and one patent. He is a member of the Editorial Board of Scientific Reports (Nature-Springer) and serves as a Reviewer for several journals. His research interests include photonic crystals, plasmonic nanostructures, optical and microwave graphene-based devices, and smart antennas.

VALERIA MARROCCO received the M.Sc. and Ph.D. degrees in electronic engineering from the Politecnico of Bari, in 2003 and 2007, respectively. Since 2007, she has been a Researcher with the Politecnico of Bari, where her research activities involved the design of photonics and nano-technology-based devices. She was also a Lecturer Assistant and Students' Supervisor. Since 2011, she has moved at CNR-ITIA (now CNR-STIIMA), where she is currently part of the research group MEDIS. She is involved in research activities concerning micro-manufacturing of micro-components and devices, related to micro-EDM and micro additive manufacturing, and to the development of monitoring systems and modeling techniques. She has coauthored several peer-review articles and took part to different national projects.

DARIO LANEVE received the M.Sc. degree *(summa cum laude)* in information engineering from the Polytechnic University of Bari, in 2014, where he is currently pursuing the Ph.D. degree in electrical and information engineering. His main research interests include microwave resonators for linear particle accelerators, microwave antennas, and fiber optic micro-resonators.

SAVINO PETRIGNANI received the B.Sc. degree in electronic and telecommunication engineering in 2015, and the M.Sc. degree in electronic engineering from Polytechnic University of Bari, Italy, where he is currently pursuing the Ph.D. degree in electrical and information engineering. His main research interests include the study of mixed-signal integrated systems and of front-end electronics for silicon photomultiplier detectors (SiPM).

FRANCESCO PRUDENZANO received the Ph.D. degree in electronic engineering, in November 1996. Since 2018, he has been a Full Professor of Electromagnetic Fields with the Department of Electrical and Information Engineering, Polytechnic University of Bari. His research activity regards the design and characterization of microwave devices, integrated optics, and optical fiber-based devices. He was a Chair of SIOF, the Italian Society of Optics and Photonics (Italian branch of European Optical Society), from 2017 to 2018. He is involved in several national and international research projects and cooperations. He has coauthored over 410 publications, 320 of which published on journals and international conferences, lectures and invited articles.

IRENE FASSI received the M.Sc. degree in mechanical engineering from Politecnico di Milano, in 1997, and the Ph.D. degree in industrial technologies, in 2001. Since 1998, she has been a full time Researcher with CNR-ITIA (now CNR-STIIMA), where she founded and leads the research group MEDIS. She is an Adjunct Professor with the University of Brescia and Politecnico di Milano for robotics, precision engineering, and advanced manufacturing systems. She is a member of the Executive Board of SIRI (Italian Robotics and Automation Association), the AITeM (Italian Association of Manufacturing Technologies), and the ASME/DED Technical Committee on Micro and Nano Manufacturing. She serves as the President elect for the International Institution for Micro-Manufacturing.